International Journal of Fatigue 118 (2019) 307–315

Contents lists available at ScienceDirect

International Journal of Fatigue

journal homepage: www.elsevier.com/locate/ijfatigue

Effects of post-processing on the thermomechanical fatigue properties of laser modified NiTi

B. Panton[a], A. Michael[a,*], Y.N. Zhou[a], M.I. Khan[b]

[a] Centre for Advanced Materials Joining (CAMJ), University of Waterloo, 200 University Avenue West, Waterloo, ON N2L 3G1, Canada
[b] Smarter Alloys, Inc., 75 Bathurst, Waterloo, ON N2V 1N2, Canada

ARTICLE INFO

Keywords:
NiTi
Shape Memory Alloy (SMA)
Laser processing
Microstructure
Fatigue

ABSTRACT

The multifunctional capabilities needed for advanced shape memory alloys (SMA) actuators has been shown to be achievable by locally tuning the properties through laser processing. Before the wide-spread use of these SMAs is realized, a detailed understanding on the long-term stability and functional life span of these material must be achieved. The current study systematically investigates the effects of thermomechanical treatment on laser modified NiTi wires, while comparing them to the original base material. Surface analysis was done using a scanning electron microscope (SEM), while microstructure analysis was performed using transmission electron microscopy (TEM). Mechanical properties were assessed using standard tensile tests and a custom built thermomechanical fatigue. Results showed that the coarse-grains, large inclusions and surface defects associated with as laser modified NiTi resulted in reduced mechanical performance. However, subsequent thermomechanical treatment restored the refined microstructure and mechanical performance similar to the base material while providing the added functionality, thus allowing for laser processed NiTi to be used for manufacturing multiple memory NiTi actuators.

1. Introduction

Development of advanced materials such as shape memory alloys drives the next industrial revolution [1,2]. These materials are used heavily in the medical and aerospace fields, and are seeing greater use as actuators across all industries [1,3–5]. Their shape memory properties are key to creating new devices that were not previously possible. When these materials were initially developed they generally required only a few cycles of transformation where fatigue was not a problem, for applications such as orthodontic archwire [4], or a press-fit seal on a jet engine [5]. Relatively recent advancements in manufacturing of SMAs coupled with a greater understanding of the evolution of the material characteristics has led to the breakthrough of SMA actuators that can undergo millions of thermomechanical cycles before failure [6,7].

There are a limited number of investigations into the thermomechanical fatigue of NiTi; due in part to the materials previous inability to reach high fatigue cycles. The benefits offered by SMA actuators over standard actuation devices have led to a rapid growth in the demand for SMA actuators by many sectors of industry [1–3]. This in turn has led to a recent increase in the investigation of the thermomechanical fatigue of SMAs [8–20], which was previously dominated by industry led research [6,7].

The next generation of SMA manufacturing will produce components with multiple embedded phase transformations creating multifunction materials [21–26]. Laser processing of SMAs is a key advancement in this area, which enables the local modification of properties through the alteration of the bulk chemistry in a confined region [21,22]. This has been used to create multiple memory actuators [21,22], monolithic materials with multiple pseudoelastic plateaus [23], self-biasing actuators [27] and many other novel devices including the SmartArch™, a revolutionary orthodontic device. The only prior work on the effects of a pulsed laser on the thermomechanical fatigue of SMA wires was Panton et al.'s [28] study on laser welded NiTi. The current work presents the initial investigation of the thermomechanical fatigue of SMA wires that have been laser processed in order to tune the local composition, as well as the ability of a cold-work and heat treatment regimen to improve thermomechanical fatigue lifespans of laser processed material and make them comparable to commercially available material.

* Corresponding author.
E-mail address: a2michae@uwaterloo.ca (A. Michael).

https://doi.org/10.1016/j.ijfatigue.2017.11.012
Received 30 May 2017; Received in revised form 29 September 2017; Accepted 26 November 2017
Available online 02 December 2017

2. Experimental procedures

2.1. Materials and processing

The materials used in this investigation were a NiTi wire from Dynalloy Inc. with a diameter of 0.38 mm that was martensitic at room temperature. The 0.38 mm wire did not undergo any further processing before testing was performed, and is referred to as D38 for the remainder of the article. This wire is used for a comparison of the performance of the laser processed wires described below.

Additionally, a NiTi wire from Furukawa Electric Co. LTD. with a diameter of 700 μm that was pseudoelastic at room temperature was also used. This wire was modified to remove Ni and make the material martensitic at room temperature. Prior to processing no oxide removal was required, as it had previously been removed by the supplier [29]. The wire was cleaned with a regimen of acetone, ethanol, and water. Laser processing was performed in an university test lab using a Miyachi Unitek LW50A pulsed Nd:YAG laser, with a wavelength of 1.064 μm and a nominal spot size of 600 μm. The melt pool created was ~1100 μm in length and penetrated the entire thickness of the wire. The wire was advanced ~440 μm in between each laser pulse to ensure complete melting of the laser processed region. A schematic of the laser process is shown in Fig. 1. During laser processing care was given to avoid excessive oxidation using argon gas shielding (flow rate of 25 CFH); however, slight surface oxidation was observed afterwards. The wires will be referred to as laser processed (LP) for the remainder of this study.

A set of the laser modified wires were subjected to a thermomechanical treatment process to reduce the grain size and reorient the texture [30,31]. The wires were solutionized at 1000 °C for 3600 s followed by a water quench. Then they were cold worked through a series of reductions, with an interannealing temperature of 600 °C for 600 s, a total area reduction of 45% after interannealing and a final heat treatment at 400 °C for 3600 s. These wires had a final diameter of 0.46 mm and are referred to as the treated laser processed (T-LP) wires.

2.2. Phase and fracture analysis

An Olympus BX51M was used for optical microscopy. A JEOL 2010F TEM/STEM field emission microscope operating at 200 kV and a Phillips CM12 analytical TEM operating at 120 kV were used for TEM analysis. Fracture analysis was performed using a JEOL JSM-6460 SEM operated at 20 kV.

Differential Scanning Calorimetry (DSC) analysis was performed with a TA Discovery DSC equipped with a refrigerated cooling system. The DSC data was recorded from −75 °C to 120 °C using a controlled heating/cooling rate of 5 °C/min. Analysis of the data was done using the TA Instruments Trios software v3.2 per the ASTM F2004-05(2010) standard.

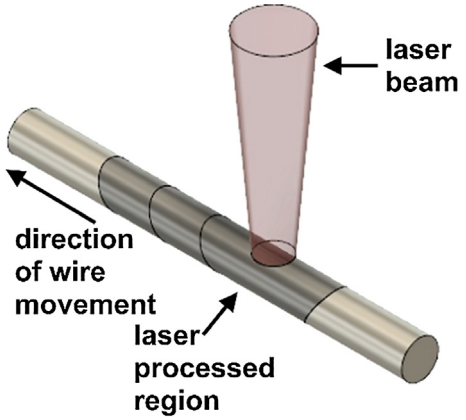

Fig. 1. Schematic depicting laser processing method.

2.3. Mechanical and thermomechanical testing

Tensile testing was performed using an Instron model 5548 microtensile tester that had a measurement accuracy of ± 0.5 μm. An ASTM F216-07 test standard with extension rate of 1.0 mm/min and a gauge length of 25.1 mm were used to test specimens.

Thermomechanical fatigue was performed using a custom setup as shown in Fig. 2. Lead weights were used to subject a constant load (shown in Table 1) that was equivalent to a 600 MPa stress based on the nominal wire diameter. A gauge length of 25.1 mm was used for testing. The grips were faced with sacrificial pieces of ceramic to ensure there was no heatsink effect on the wire. The heating was performed at constant currents controlled by a Sorensen XG 33-25 power supply. These currents were set according to the recommended currents by Dynalloy Inc. for wires of these diameters, as shown in Table 1. The current for the 0.70 mm diameter laser processed wire was determined by extrapolating the data provided by Dynalloy Inc. The current was delivered by speaker posts, shown in Fig. 2. Heating was controlled to specific strain and thermally cycled until failure. Cooling was performed using a vortex tube that was turned on when the current was turned off. Cooling stopped and heating was initiated once the change in slope of the displacement was less than 0.0001 mm, which was less than 0.04% of the total strain, or what served as the benchmark for 0 in these tests. The vortex tube had a nozzle attachment that constricted the air to blow along the entire gauge length of the test wire, ensuring rapid and uniform cooling. The setup measured the load using an Omega LCMFD 500 N load sensor and the displacement using a MT 2571 Heidenhain displacement sensor with a measurement sensitivity of ± 0.2 μm. A NI PXI-1031 DAQ from National Instruments was used to monitor the sensors and control the power supply.

3. Results and discussion

3.1. Microstructure

The laser processing technique implemented in this study fully remelted the work material. The centreline of the laser processed fusion zone was the weak point where failure occurred during initial wire drawing attempts. To avoid this, the fusion zone centrelines were partially removed by overlapping the laser processed spots by 60%. The entire centreline could not be removed by increasing the overlap percentage, because this would result in an increase in Ni vaporization that would lead to Ti saturation and the formation of large amounts of Ti_2NiO_x phases. The laser processed microstructure is shown in Fig. 3. The microstructure of the LP material is very coarse, with the grains and dendrites in the micron scale. Both the fusion boundary and the remaining centreline can be observed with the fusion zone being predominantly large columnar dendrites (see Fig. 3), which is typical of welded NiTi wires [29,32]. There is also a thin region of planar growth at the fusion boundary. Due to the relatively small cross-sectional area of the wires, heat conduction away from the melt pool is restricted, which impedes the cooling rate in the fusion zone. The result is the planar growth at the fusion boundaries and the columnar dendrites in the fusion zone [29,33,34]. Epitaxial growth is also observed, as indicated by the dendritic grain that cross the fusion boundary (see Fig. 3).

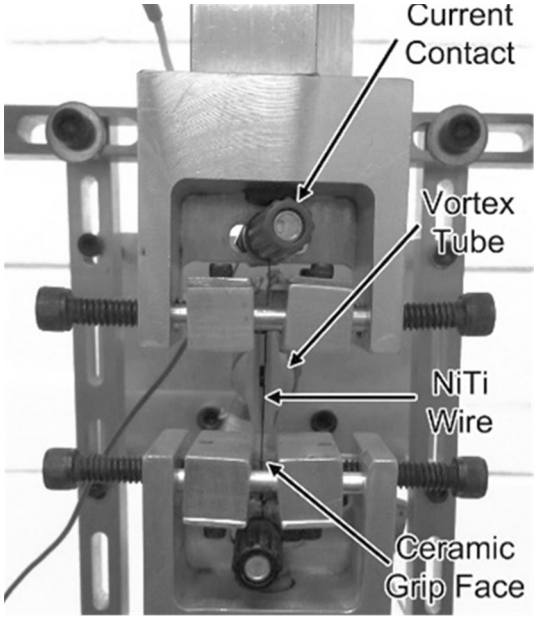

Fig. 2. Thermomechanical fatigue tester.

Table 1
Wire diameter, loads and currents used in the thermomechanical fatigue tests.

Wire	LP	T-LP	D38
Nominal diameter (μm)	700	460	381
Constant load (N)	241	100	68
Current (A)	7.43	3.27	2.25

TEM analysis of the LP sample is shown in Fig. 4. The diffraction pattern shown in Fig. 4a indicates that the material was in the B19′ phase at room temperature. Fig. 4b shows a large amount of Ti_2NiO_x present, due to the saturation of Ti in the matrix. Compositional analysis was used to confirm the identity of these inclusions. The Ti_2NiO_x phase was formed by microsegregation along the boundaries of the dendrites [35,36]. It should be noted that these inclusions may be the result of oxide entrapment, the source of which could either be from the atmosphere (i.e. insufficient shielding) or pre-existing oxide on the sample surface. This material exhibited type I and type II twins, which is typical of larger grain sizes [37,38].

In comparison, the microstructure of the T-LP samples was a refined nanograined material, as shown in Fig. 5. The material appears to be primarily R-phase; however, the regions with dark contrast (see Fig. 5a) may correspond to nanograins of martensite [39]. The average grain size measured via dark-field imaging was 29 nm. This is confirmed by the presence of continuous diffraction rings (see Fig. 5a), which indicates the material is nanocrystalline with grains between 20 and 70 nm [39]. This grain size geometrically constricts the matrix such that the compound (0 0 1) twinning of nanoscale microstructures form (see Fig. 5c) [37]. These compound twins have a much higher density compared to the larger scale type I and type II twins (see Fig. 4c) of the coarser microstructure that was observed in the LP sample [38]. During wire drawing, the Ti_2NiO_x inclusions were fractured and created particle-void-assemblies, as shown in Fig. 5b.

TEM analysis of the microstructure of the D38 sample is shown in Fig. 6. The material appears to be R-phase with an average grain size as measured by dark-field TEM of 72 nm. The presence of a discrete diffraction ring again confirms nanocrystallinity, while the diffuse surroundings suggest partial amorphization [39]. This partial amorphization is likely due to the training regimen performed by the manufacturer, since it has been shown that deformation of NiTi SMAs results in localized amorphization [40]. This Ti-rich material had no observed Ni_4Ti_3 precipitates, as these do not form in Ti-rich NiTi. Furthermore, no Ti_2NiO_x and TiC inclusions were found in the TEM sample.

3.2. Surface properties

The surface properties of NiTi can affect the fatigue life of components [30]. This effect can become significant at smaller cross-sectional sizes where defects become proportionally larger, and where the surface region becomes a large fraction of the cross-sectional area [30]. Fig. 7 shows the SEM images of the surface of the LP, T-LP and D38 wires. Large cracks in the solidification surface are seen in the laser processed specimens, while the dominant feature in the wire drawn specimens is the striations. Qualitatively the T-LP wires are very similar to the D38 wires from the industry supplier. It follows that the effects of this surface would be similar to those seen in the industrial material.

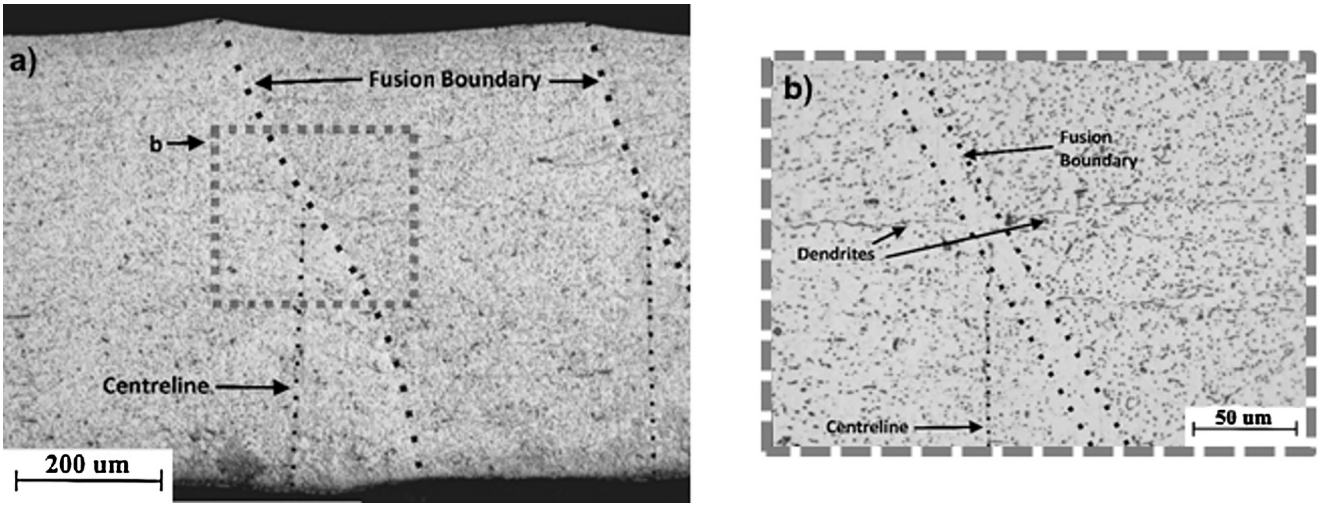

Fig. 3. Optical micrograph of (a) laser processed NiTi cross section and (b) close-up of centerline partially overlapped by fusion zone.

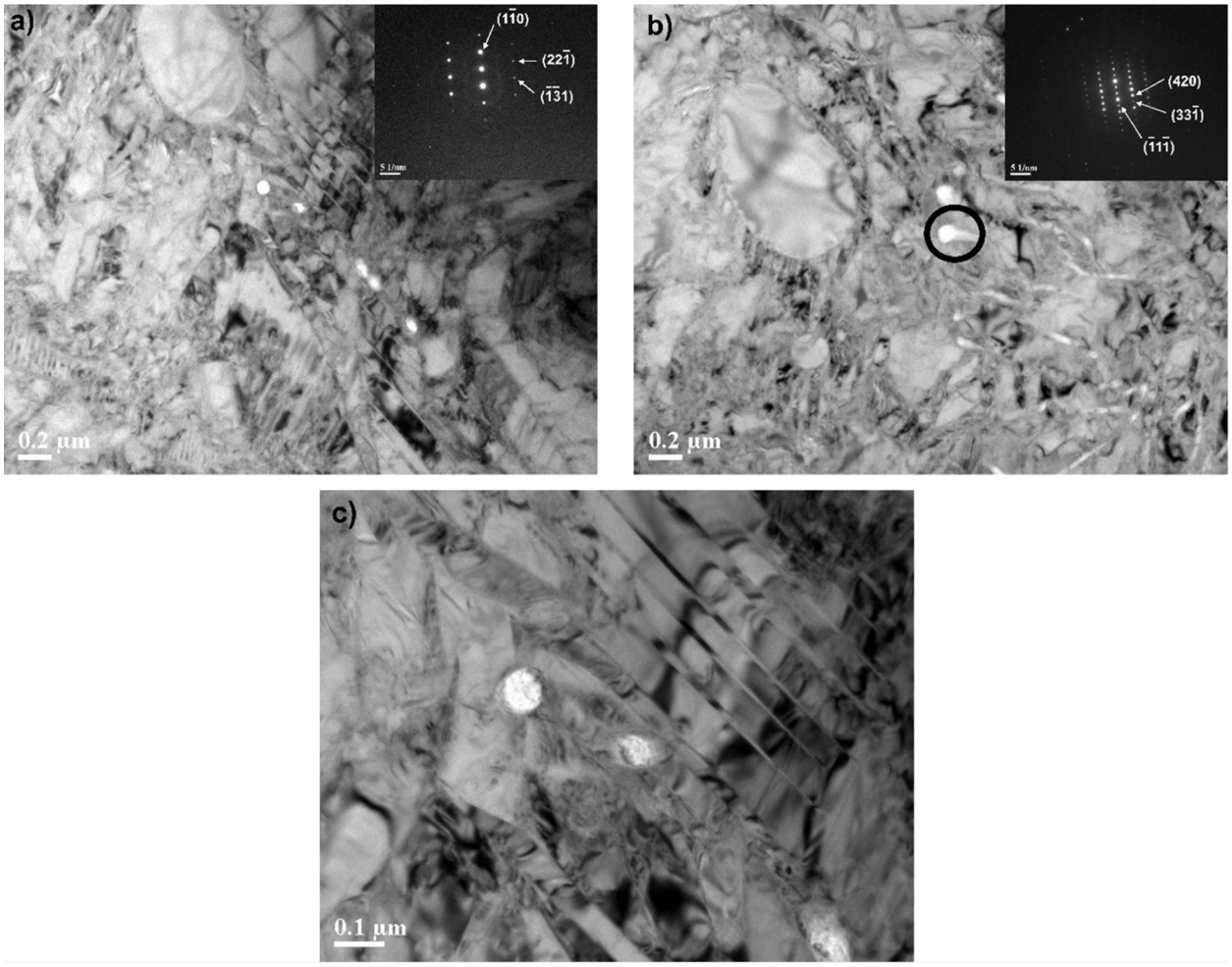

Fig. 4. TEM (a) of the LP twinned matrix, (b) Ti_2NiO_x phase with in the matrix, (c) close-up of the twin morphology.

3.3. Thermal and physical properties

The DSC results are shown in Fig. 8. The LP sample has a single-phase transformation typical of coarse-grained, low dislocation density and unprecipitated NiTi [41]. The T-LP and D38 samples had similar phase transformation properties to one another. They had a multi-stage phase transformation of a nanograined microstructure which geometrically constrained the martensite, reducing the maximum transformation strain, leading to the lower strain transformation of the R-phase [42]. The peaks of both these materials are in similar positions, indicating that they have similar compositions, microstructures, and exhibit R-phase at room temperature, which is confirmed by the TEM analysis discussed in the previous section. The sharp peaks of the T-LP phase transformations indicate that the grains were dislocation lean [43]. The broad peaks of the D38 phase transformations indicate that the material had undergone training by the manufacturer to stabilize the microstructure by introducing dislocations to create networks [44,45].

The results of the tensile test pull-to-failure are displayed in Fig. 9. The coarse-grained microstructure of the LP sample resulted in a lower UTS and ductility compared to the nanocrystalline T-LP sample. The T-LP and D38 had the same UTS, while the T-LP had a 34% greater ductility than the D38, due to the smaller grain size [46]. It is also important to note that D38 sample experienced a very low reorientation stress (~15 MPa) due to previous training performed by the manufacturer. However, both of the laser processed samples experienced higher reorientation stresses. The reorientation stress for the LP sample is ~250–300 MPa, which is typical for an untrained NiTi wire that is being strained well below the martensite start temperature [47]. Additionally, the reorientation stress for the T-LP sample is ~100 MPa, which is typical for an untrained NiTi wire that is being strained above the martensite start temperature but below the austenite finish temperature [47].

Additionally, the materials were tensile cycled to a load of 600 MPa and then thermally cycled at zero stress to recover shape memory strain, as shown in Fig. 10. The coarse-grained LP sample had a significant plastic strain, and the ensuing plastic deformation resulted in a shape memory strain that was only 18% the amount of the D38 material after 10 cycles. The T-LP sample had an increase in plastic strain compared to the LP sample, but achieved a shape memory strain equal to that of the D38 material. The smaller grains enabled a larger amount of deformation to occur than the coarser LP sample, but a significant part of this deformation was not recoverable due to the constriction of the matrix [48,49] and possibly in part to the presence of the particle-

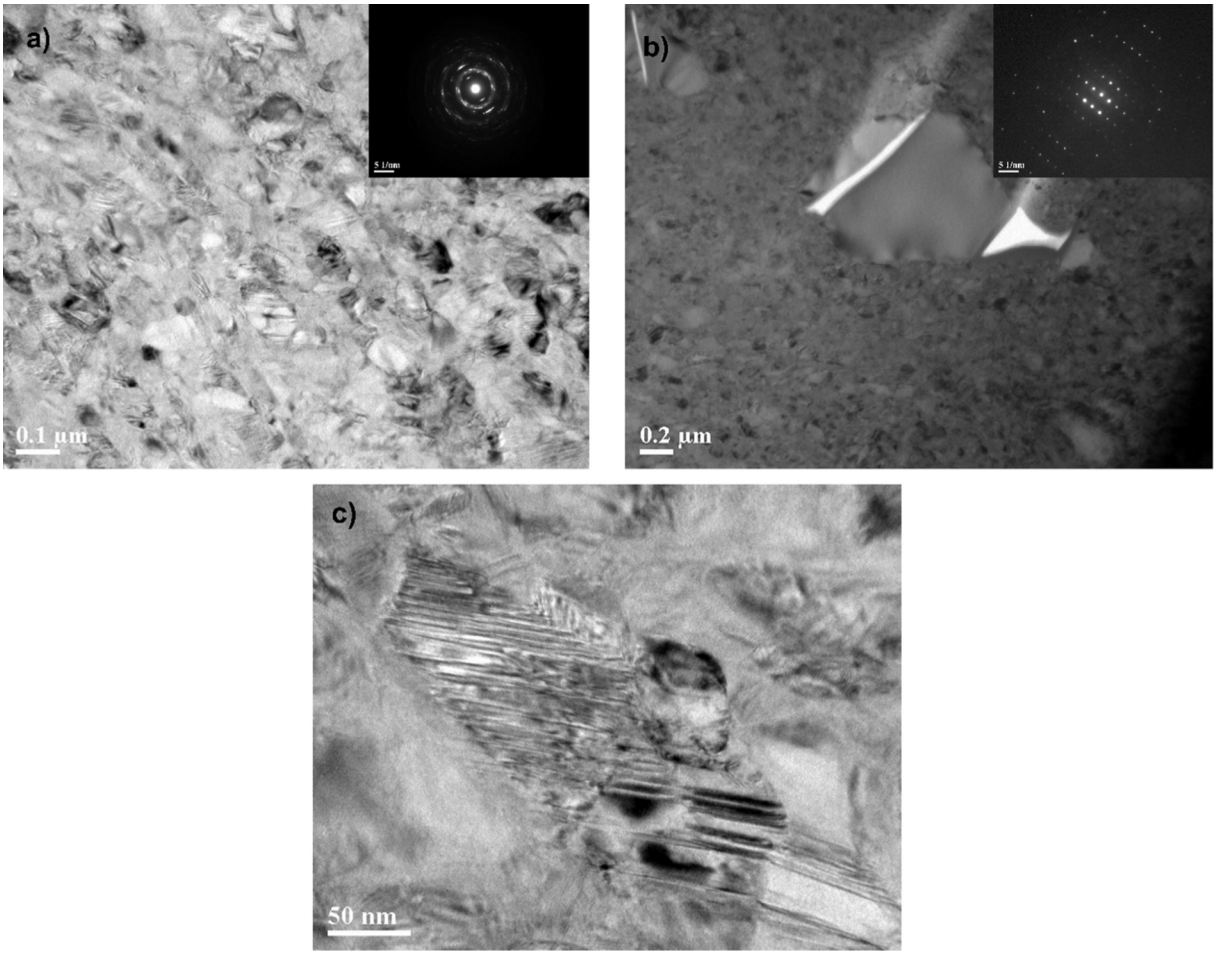

Fig. 5. TEM of (a) of the T-LP matrix, (b) Ti_2NiO_x particle void assembly and (c) close-up of the twin morphology.

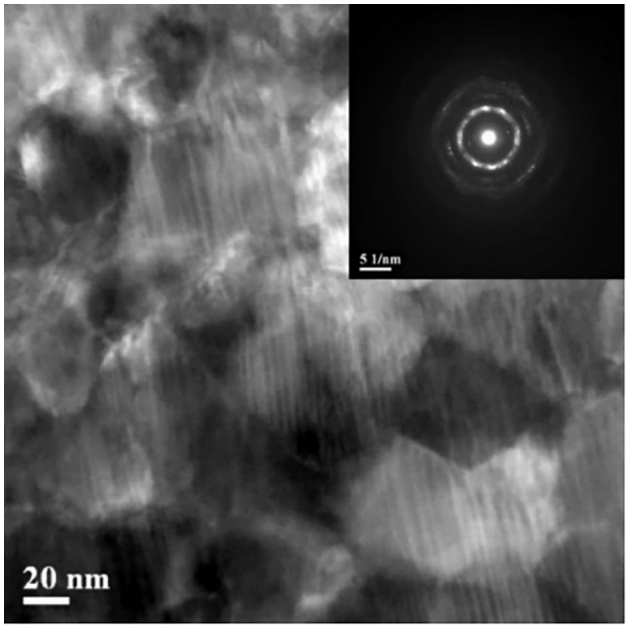

Fig. 6. TEM of the nanocrystalline microstructure of the D38 sample.

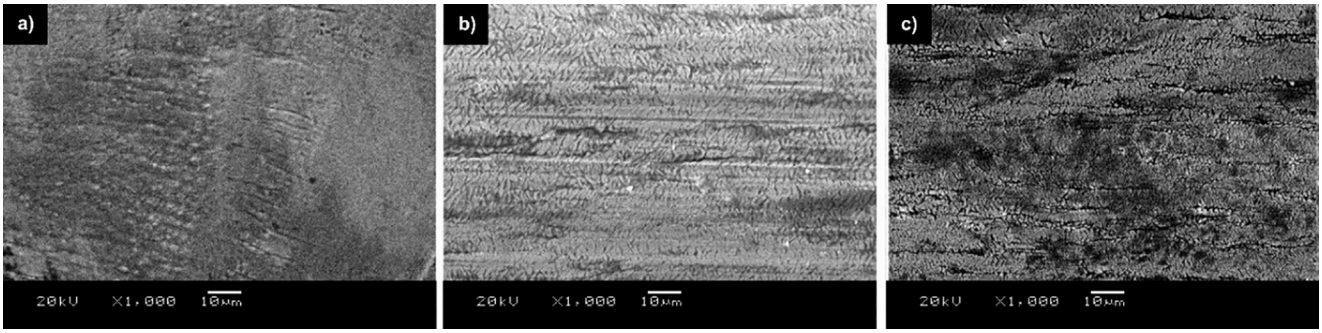

Fig. 7. Surface of (a) LP, (b) T-LP and (c) D38.

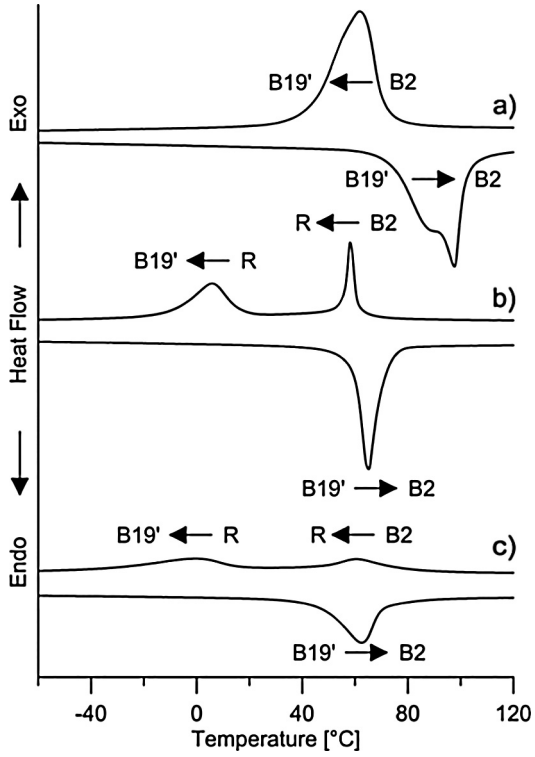

Fig. 8. DSC analysis of (a) LP, (b) T-LP and (c) D38.

void-assemblies. The D38 wire had only 22% of the plastic strain build-up that the T-LP sample experienced, but a similar shape memory strain. The training that the D38 material had undergone was used to build a dislocation network that ensured it would have a more stable initial deformation than the virgin, untrained T-LP sample, which was dislocation lean as indicated by the DSC curves in Fig. 8.

3.4. Thermomechanical fatigue properties

Comparison of the fatigue lives of the LP, T-LP, and D38 are shown in Fig. 11. The wires were loaded to 600 MPa and thermally cycled to controlled strains until failure. The coarse-grained LP sample was previously shown to have high plastic build-up and low shape memory strain which resulted in extremely low fatigue lives compared to the T-LP and D38 samples. The thermomechanical fatigue life of NiTi is related to the maximum achievable strain [12,30]. The lower the percentage of the maximum strain used, the greater the fatigue life achievable. The maximum strains for 1 cycle at a load of 600 MPa are indicated on the strain axis (i.e. Y-axis) of Fig. 11. The microstructure of the D38 material facilitated the maximum recoverable strain, followed by the more restricted, smaller grained T-LP sample, and finally the coarse-grained LP sample. At lower percentages of the maximum strain the T-LP and D38 had fatigue lives in the same order of magnitude.

The T-LP exhibited a substantial increase in both achievable strains and fatigue life at these higher strains compared to the LP sample. D38 showed a further increase in both achievable strain and fatigue life due to the more preferential grain size [12], and the training that it underwent by the manufacturer [44,45]. The presence of particle-void-assemblies may have contributed to the reduced fatigue life observed in the T-LP samples when compared with the D38 sample. However, a training regime of 20 cycles at 4% strain was applied to the T-LP material and resulted in an increase in the fatigue life from 21,474 cycles to 33,043 cycles at 2% strain, which brings it close to parity with the D38 material that had an average cycle life of 36,022 cycles at 2% strain, as shown in Fig. 11. The stability of the microstructure ensured that progression of dislocations, and crack growth was slowed in the trained T-LP material, leading to the longer fatigue life than the LP material [12,30].

SEM images of the fatigue fractures are shown in Fig. 12. The LP sample experienced a ductile rupture type failure that can be observed across the entire fracture surface, as shown in Fig. 12a. The coarse-grained and dislocation lean material with large inclusions underwent significant transformation induced plasticity in a small number of cycle, leading to this ruptured surface [8–12]. The T-LP and D38 samples have a small, distinct region where the crack initiated and propagated (see Fig. 12b and c), with most of the surface having ductile rupture properties. The nanocrystalline material impeded the dislocation activity of transformation induced plasticity, delaying crack initiation in these materials [50–52]. The majority of high cycle fatigue life in NiTi is in the crack initiation stage, with propagation occurring rapidly once the critical crack size is reached [53], which accounts for the uniformity of the fracture surfaces in Fig. 12b and c. This suggests that the presence of the particle-void-assemblies observed in the T-LP material may not have contributed to reduced fatigue life unless they were near the surface, since brittle inclusions located at the surface serve as the crack initiation points [54].

4. Conclusions

Although the laser modified material exhibited reduced mechanical performance, subsequent thermomechanical treatment aided in

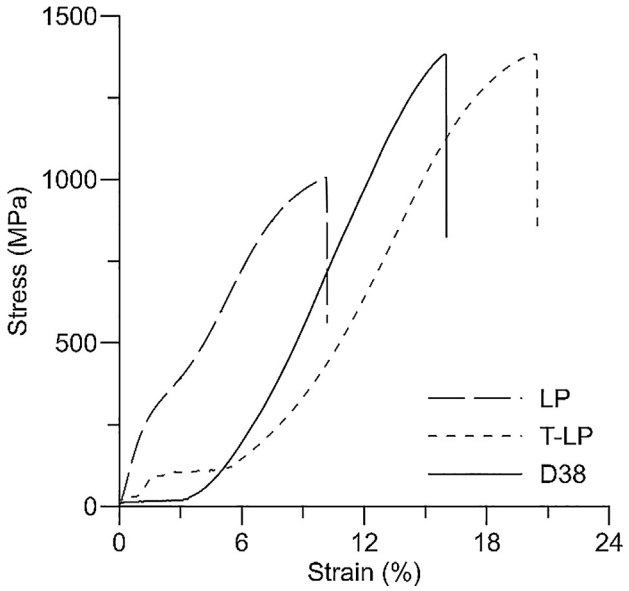

Fig. 9. Tensile test pull-to-failure of the LP, T-LP and D38 at room temperature.

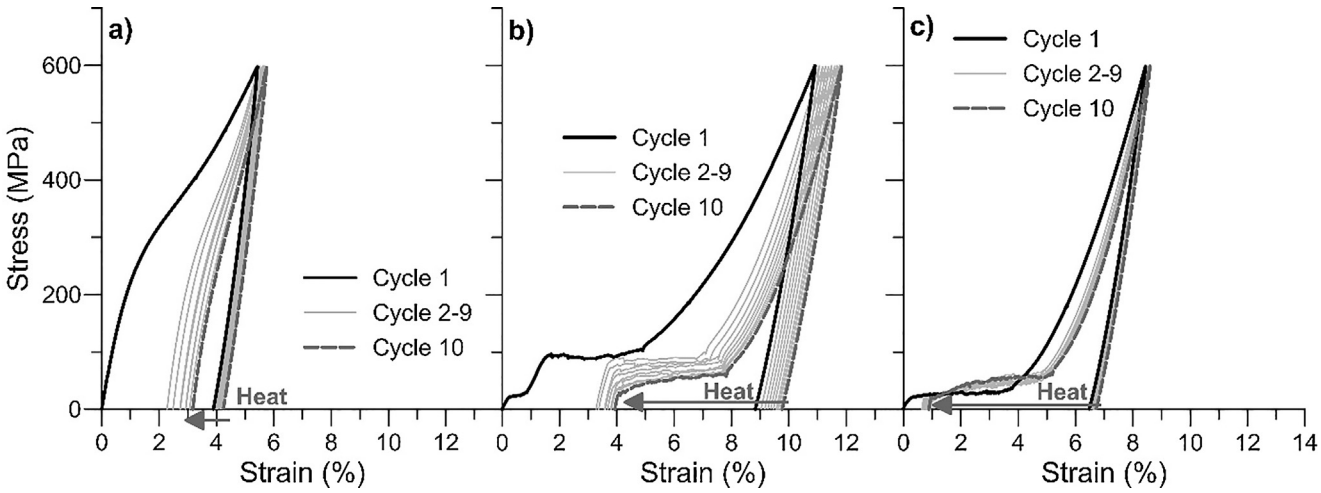

Fig. 10. Tensile cycling to 600 MPa at room temperature, and zero-load shape memory recovery of (a) the LP sample, (b) the T-LP sample and (c) the D38 sample.

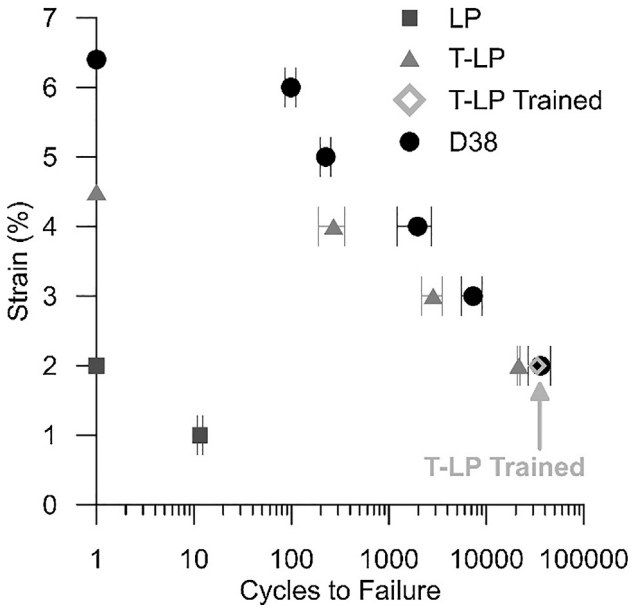

Fig. 11. Cycles to failure of LP, T-LP, trained T-LP and D38 loaded to a constant 600 MPa and cycled to the indicated strains.

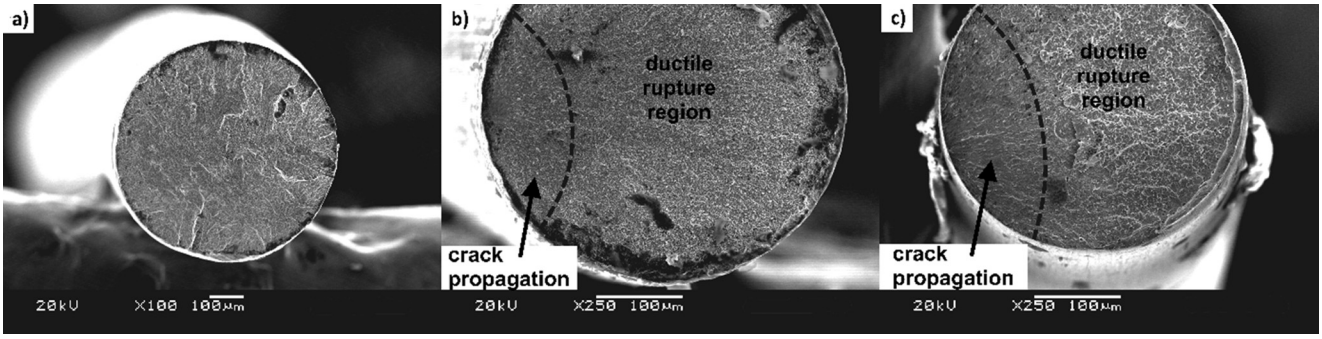

Fig. 12. SEM images of fracture surfaces for (a) LP (at 0.5% strain), (b) T-LP (at 2% strain) and (c) D38 (at 2% strain) after cyclic fatigue testing.

restoring the properties while maintaining the added functionality. The T-LP material had the same UTS as the D38, but 34% greater ductility due to the smaller grain size. Also, the T-LP had the same shape memory recovery strain as D38 when cycled to 600 MPa and thermally recovered at zero-load, however, the T-LP showed a 347% greater plastic strain when compared to D38. The training of the D38 material by the manufacturer, and the less constrictive microstructure (slightly larger grains) of the D38 material ensured lower permanent deformation compared to the T-LP.

When loaded to 600 MPa, the coarse-grained and embrittled LP material had 1/3 of the recoverable strain of D38 and fatigue lives that were orders of magnitudes smaller. The T-LP had 2/3 of the maximum achievable strain of the D38, and fatigue lives in the same order of magnitude as D38 at the lower strain values. The smaller grain size of the T-LP material limited the achievable strain. Training of the treated laser processed NiTi increased the fatigue life to parity with the D38 at 2% strain. The current work demonstrates the feasibility of using laser processing to tune the local material composition and post-process thermomechanical treatments to match the mechanical properties of commercially available alloys. Future work is underway to optimize the processing and training of laser modified NiTi to achieve superior fatigue properties for multifunctional actuators.

Acknowledgements

The authors would like to acknowledge the support of the Natural Sciences and Engineering Research Council of Canada (www.nserc.ca), the Canada Research Chairs Program (www.chairs-chaires.gc.ca) and the Ontario Centres of Excellence (http://www.oce-ontario.org/). The expertise and technical support of the Canadian Centre for Electron Microscopy (CCEM, ccem.mcmaster.ca), Smarter Alloys Inc. (smarter-alloys.com) and the Microwelding, Medical and Smart Materials Processing group of the Centre for Advanced Materials Joining (CAMJ, mme.uwaterloo.ca/~camj/) at the University of Waterloo were also essential to the completion of this study.

References

[1] Mohd Jani J, et al. A review of shape memory alloy research, applications and opportunities. Mater Des 2014;56:1078–113.
[2] Elahinia MH, et al. Manufacturing and processing of NitI implants: a review. Prog Mater Sci 2012;57:911–46.
[3] Butera F. Shape memory actuators for automotive applications. Adv Mater Processes 2008;166:37–40.
[4] Duerig T, Pelton A, Stöckel D. An overview of nitinol medical applications. Mater Sci Eng, A 1999;273–275:149–60.
[5] Hartl DJ, Lagoudas DC. Aerospace applications of shape memory alloys. Proc Inst Mech Eng, Part G: J Aerosp Eng 2007;221:535–52.
[6] Tuissi A, et al. Fabrication process and characterization of NiTi wires for actuators. Milano, Italy: SAES Getters; 2004.
[7] Fumagalli L, Buters F, Coda A. SmartFlex® NiTi wires for shape memory actuators. J Mater Eng Preform 2009;18:691–5.
[8] Bhaumikm SK, Ramaiah KV, Saikrishna CN. Nickel-titanium shape memory alloy wires for thermal actuators. In Vinoy KJ, editor. Micro and smart devices and systems. India: Springer; 2014. p. 181–98.
[9] Kockar B, et al. Thermomechanical cyclic response of an ultrafine-grained NiTi shape memory alloy. Acta Mater 2008;56:3630–46.
[10] Saikrishna CN, et al. Influence of stored elastic strain energy on fatigue behavior of NiTi shape memory alloys. Mater Sci Eng, A 2013;587:65–71.
[11] Wurzel D. Effects of different thermomechanical treatments on fatigue of NiTi shape memory alloys. J De Physique IV 2001; 11: Pr8-535-Pr8-540.
[12] Frenzel J, et al. Improvement of NiTi shape memory actuator performance through ultra-fine grained and nanocrystalline microstructures. Adv Eng Mater 2011;13:256–68.
[13] Gall K, et al. Effect of microstructure on fatigue of hot-rolled and cold-drawn NiTi shape memory alloys. Mater Sci Eng, A 2008;486:389–403.
[14] Belyaev S, Resnina N, Sibirev A. Peculiarities of the residual strain accumulation during thermal cycling of TiNi alloy. J Alloy Compd 2012;542:37–42.
[15] Wu X, Kutschej K, Kneissi AC. Study on the thermal fatigue of NiTi wires. Zeitschrit fur Metallkunde 2003;94:122–6.
[16] Meier H, et al. Smart control systems for smart materials. J Mater Eng Perform 2011;20:559–63.
[17] Casati R, Tussi A. Effect of current pulses on fatigue of thin NiTi wires for shape memory actuators. J Mater Eng Perform 2012;21:2633–7.
[18] Ramaiah KV, et al. Fracture of thermally activated NiTi shape memory alloy wires. Mater Sci Eng, A 2011;528:5502–10.
[19] Lagoudas DC, et al. Thermomechanical fatigue of shape memory alloys. Smart Mater Struct 2009;18:1–12.
[20] Scirè Mammano G, Dragoni E. Functional fatigue of Ni-Ti shape memory wires under various loading conditions. Int J Fatigue 2014;69:71–83.
[21] Khan MI, Pequegnat A, Zhou YN. Multiple memory shape memory alloys. Adv Eng Mater 2013;15:386–93.
[22] Pequegnat A, et al. Local composition and microstructure control for multiple pseudoelastic plateau and hybrid self-biasing shape memory alloys. Mater Des 2015;92:802–13.
[23] Michael A, Zhou YN, Khan MI. Experimental validation of a one-dimensional model for monolithic shape memory alloys with multiple pseudoelastic plateaus. J Intell Mater Syst Struct 2016;27:2102–11.
[24] Bellouard Y, et al. Local annealing of complex mechanical devices: a new approach for developing monolithic micro-devices. Mater Sci Eng, A 1999;273–275:795–8.
[25] Meng Q, et al. Functionally graded NiTi strips prepared by laser surface anneal. Acta Mater 2012;60:1658–68.
[26] Scherngell H, Kneissl AC. Generation, development and degradation of the intrinsic two-way shape memory effect in different alloys systems. Acta Mater 2002;50:327–41.
[27] Panton B, Zhou YN, Khan MI. A stabilized, high-stress self-biasing shape memory alloy actuator. Smart Mater Struct 2016;25.
[28] Panton B, et al. Thermomechanical fatigue of post-weld heat treated NiTi shape memory alloy wires. Int J Fatigue 2016; 92(Part 1): p. 1–7 [11].
[29] Tam B, Khan MI, Zhou YN. Mechanical and functional properties of laser-welded Ti-55.8 wt pct Nitinol wires. Metall Mater Trans A 2011;42A:2166–75.
[30] Robertson SW, Pelton AR, Ritchie RO. Mechanical fatigue and fracture of Nitinol. Int Mater Rev 2012;57:1–37.
[31] Pelton A. Nitinol fatigue: a review of microstructures and mechanisms. J Mater Eng Perform 2011;20:613–7.
[32] Lin HC, Wu SK, Lin JC. The martensitic transformation in Ti-rich TiNi shape memory alloys. Mater Chem Phys 1994;37:184–90.
[33] Chan CW, Man HC, Cheng FT. Fatigue behavior of laser-welded NiTi wires in small-strain cyclic bending. Mater Sci Eng, A 2013;559:407–15.
[34] Kou S. Welding metallurgy. Hoboken, NJ: John Wiley Sons Inc; 2003.
[35] Schuessler A, Haas T, Schlossmacher P, Borgmann H. Micro welding of NiTi shape memory alloys. In: Proc actuator 94: 4th internat conf on new actuators, Bremen; June 15–17, 1994. p. S. 372–376.
[36] Sczerzenie F, Manjeri RM, Belden C, LaFond R. The effect of alloy formulation, cold work and inclusion content on micro-void formation in NiTi alloys. In: The international conference on Shape Memory and Superelastic Technologies (SMST) May 12-16, Pacific Grove, California, USA; 2014. p. 17.
[37] Waitz T, Spisak S, Hafner J, Karnthaler HP. Size-dependent martensitic transformation path causing atomic-scale twinning of nanocrystalline NiTi shape memory alloys. Europhys Lett 2005;71:98–103.

[38] Waitz T, Kazykhanov V, Karnthaler HP. Martensitic phase transformations in nanocrystalline NiTi studied by TEM. Acta Mater 2004;52:137–47.
[39] Sharifi EM, Kermanpur A, Karimzadeh F, Esmaili A. Formation of nanocrystalline structure in an equiatomic NiTi shape-memory alloy by thermomechanical processing. J Mater Eng Perform 2014;23:1408–14.
[40] Hu L, Jiang S, Zhang Y, Zhao Y, Liu S, Zhao C. Multiple plastic deformation mechanisms of NiTi shape memory alloy based on local canning compression at various temperatures. Intermetallics 2016;70:45–52.
[41] Otsuka K, Ren X. Physical metallurgy of Ti–Ni-based shape memory alloys. Prog Mater Sci 2005;50:511–678.
[42] Waitz T, Antretter T, Fischer FD, Karnthaler HP. Size effects on martensitic phase transformations in nanocrystalline NiTi shape memory alloys. Mater Sci Technol 2008;24:934–40.
[43] Pelton AR, Huang GH, Moine P, Sinclair R. Effects of thermal cycling on microstructure and properties in Nitinol. Mater Sci Eng, A 2012;532:130–8.
[44] Saikrishna CN, Ramaiah KV, Bhaumik SK. Effects of thermo-mechanical cycling on the strain response of Ni-Ti-Cu shape memory alloy wire actuator. Mater Sci Eng, A 2006;428:217–24.
[45] Erbstoeszer B, Armstrong B, Taya M, Inoue K. Stabilization of the shape memory effect in NiTi: an experimental investigation. Scr Mater 2000;42:1145–50.
[46] Schaffer J. Structure-property relationships in conventional and nanocrystalline NiTi intermetallic alloy wire. J Mater Eng Perform 2009;18:582–7.
[47] Miyazaki S, Otsuka K, Suzuki Y. Transformation pseudoelasticity and deformation behavior in a Ti-50.5at%Ni alloys. Scr Metall 1981;15:287–92.
[48] Polatidis E, Zotov N, Bischoff E, Mittemeijer EJ. The effect of cyclic tensile loading on the stress-induced transformation mechanism in superelastic NiTi alloys: an in-situ X-ray diffraction study. Scr Mater 2015;100:59–62.
[49] Delville R, Malard B, Pilch J, Sittner P, Schryvers D. Microstructure changes during non-conventional heat treatment of thin Ni–Ti wires by pulsed electric current studied by transmission electron microscopy. Acta Mater 2010;58:4503–15.
[50] Eggeler G, Hornbogen E, Yawny A, Heckmann A, Wagner M. Structural and functional fatigue of NiTi shape memory alloys. Mater Sci Eng, A 2004;378:24–33.
[51] Saikrishna C, Ramaiah K, Allam Prabhu S, Bhaumik S. On stability of NiTi wire during thermo-mechanical cycling. Bull Mater Sci 2009;32:343–52.
[52] Melton KN. Ni-Ti based shape memory alloys. In: Engineering aspects of shape memory alloys anonymous. London: Butterworth-Heinemann; 1990. p. 21–35.
[53] Wick A, Gong XY, Fino J, Sheriff J, Pelton AR. Bending fatigue characteristics of nitinol. In: Proc ASM materials & processes for medical devices conf. Minneapolis, MN, USA; August 2004. p. 15–20.
[54] Hornbogen E. Review thermo-mechanical fatigue of shape memory alloys. J Mater Sci 2004;39:385–99.